

Thermal stability and electronic properties of amorphous Zr-Co and Zr-Ni alloys

K. H. J. Buschow and N. M. Beekmans

Philips Research Laboratories, Eindhoven, The Netherlands

(Received 19 October 1978)

Amorphous Zr-Co and Zr-Ni alloys were prepared by melt spinning over a wide range of 3*d*-metal concentrations (20%–90%). These alloys were investigated by x-ray diffraction and their crystallization temperatures were determined by differential scanning calorimetry. Magnetic and resistivity measurements were made in the range 4.2–300 K. Many of the amorphous alloys investigated were found to have a rather large electrical resistivity with a negative temperature coefficient. This property has been explained in terms of the extended Ziman theory of liquid metals. The significance of charge transfer in these alloys is discussed.

I. INTRODUCTION

Following the recognition that amorphous metals obtained by rapid quenching from the melt can have outstanding mechanical, electrical, or magnetic properties, often superior to those of crystalline materials, the preparation of new amorphous alloys and the study of their physical properties have proliferated.¹

In the present paper we report on the magnetic and electrical properties of amorphous alloys obtained by combining Zr with either Ni or Co. Also included are results of x-ray diffraction and specific-heat measurements. The interest in these alloys stems mainly from the fact that they can be obtained in the amorphous state over a very extended concentration region. Because of this they lend themselves well to a study of the changes in electronic properties with concentration and of the manner in which these changes influence the various physical properties.

II. EXPERIMENTAL

The amorphous alloy ribbons were prepared by means of the melt spinning technique in an atmosphere of purified argon. X-ray diffraction was performed on small parts of the ribbons by means of Cu *K* α radiation in combination with an x-ray monochromator. The crystallization temperatures were determined in purified argon on a differential scanning calorimeter, using a heating rate of 50 °C/min. The magnetic-susceptibility measurements were done on a vibrating-sample magnetometer. The magnetic properties of the samples relatively rich in 3*d* metal were determined by means of an adaptation of the Faraday method. The electrical resistivity was studied on small parts of the ribbons. The measurements were made quasicontinuously at slowly changing temperatures by means of a four-probe technique.

III. EXPERIMENTAL RESULTS

The x-ray diffractograms of the alloy ribbons investigated are characterized by diffuse lines similar to those shown for Zr₇₈Ni₂₂ in Fig. 1. The scattering vectors $Q_p = 4\pi \sin\theta/\lambda$ corresponding to the first broad maximum are listed for various alloys in Table I.

Two typical sets of data obtained for the alloys Zr₇₈Ni₂₂ and Zr₆₀Ni₄₀ by means of the differential scanning calorimeter are shown in Fig. 2. The exothermal crystallization process is reflected in a sharp peak in the temperature dependence of the specific heat. In several cases the first peak is followed by a second peak at slightly higher temperature (see Zr₇₈Ni₂₂ in Fig. 2). As will be shown below this indicates that the first crystalline phase is metastable and transforms into a different crystalline phase upon further heating. Both crystallization processes are irreversible, as shown by the bottom line in Fig. 2, which was obtained by cooling the samples. The temperatures corresponding to the maximum of the first peak are listed for various amorphous alloys in Table I under T_x .

In amorphous Zr₇₈Ni₂₂ we studied the crystallization process in more detail. After heating to slightly above the first crystallization peak (350 °C) the calorimetric experiment was stopped and the sample cooled quickly to room temperature. Subsequent x-ray analysis showed that the first phase crystallized is of a bcc structure (lattice constant $a = 3.572 \text{ \AA}$). In a separate run amorphous Zr₇₈Ni₂₂ was heated to a temperature well above the second peak and then cooled quickly to room temperature. X-ray diffraction now showed the presence of two crystalline phases. One of these was α -Zr, the other was the tetragonal phase Zr₂Ni (CuAl₂ type). On the basis of the Zr-Ni phase diagram a mixture of the phases Zr and Zr₂Ni is indeed expected to be in thermal equilibrium in the temperature and concentration

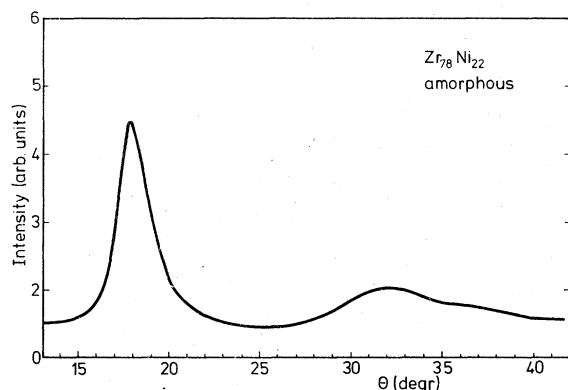


FIG. 1. X-ray diffraction diagram (Cu $K\alpha$ radiation) taken on pieces of amorphous ribbons of the alloy $Zr_{78}Ni_{22}$.

range considered.² It can be concluded therefore that the first crystallization peak corresponds to the formation of a metastable bcc phase which, at slightly higher temperatures (second peak), decomposes into two stable crystalline phases.

The magnetic properties of the amorphous alloys can be described as follows: Magnetic ordering was detected only in the alloys of relatively high $3d$ atom concentration. The values of the moment per $3d$ atom in these alloys, derived from the magnetization at 4.2 K in a field of 18 kOe, are given between parentheses in the last column of Table I. These values are significantly lower than those obtained in amorphous Y- $3d$ alloys of comparable composition.³⁻⁵ This indicates that the $3d$ moment reduction by

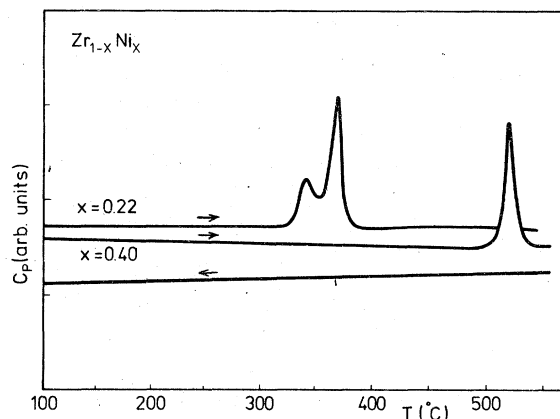


FIG. 2. Temperature dependence of the apparent specific heat of two Zr-Ni amorphous alloys obtained with increasing temperature on a differential scanning calorimeter. The lowest curve was obtained with decreasing temperature.

means of Zr is somewhat stronger than that by means of Y. The origin of the $3d$ moment reduction has been discussed elsewhere.³⁻⁵

Results of the resistivity measurements are shown in Figs. 3 and 4. The prominent feature in all these resistivity data is the rather high residual resistivity, reflecting the high atomic disorder in the amorphous materials. It can also be seen that the temperature dependence of the resistivity is rather low and does not involve the relatively large lattice contribution ($\rho \propto T$) usually encountered in crystalline materials. The resistivity of most of the alloys investigated has a

TABLE I. Scattering vectors $Q_p = 4\pi \sin \theta / \lambda$ corresponding to the first diffuse halo in various amorphous alloys. The crystallization temperatures (T_x) correspond to the maximum of the first peak in differential-scanning-calorimeter tracings. The ratios T_x/T_m were derived by means of the melting temperatures given by Elliot (Ref. 2). Instead of the magnetic susceptibility (χ) saturation moments are given (in parentheses) for those alloys showing magnetic ordering.

$Zr_{1-x}Ni_x$	Q_p (\AA^{-1})	T_x (K)	T_x/T_m	χ (10^5 emu g^{-1})
$x = 0.22$	2.50	611	0.49	0.27
$x = 0.24$	2.51	638
$x = 0.36$	2.62	730	0.57	0.2
$x = 0.60$	2.81	791	0.59	...
$x = 0.63$	2.85	839	0.63	0.2
$x = 0.90$	3.12	736	0.51	($0.16 \mu_B$ / Ni)
$Zr_{1-x}Co_x$				
$x = 0.22$	2.51	643	0.51	0.27
$x = 0.30$	2.55	700	0.56	0.25
$x = 0.36$	2.60	740	0.55	...
$x = 0.53$	2.76	785	0.50	1.37
$x = 0.90$	3.07	833	0.56	($1.37 \mu_B$ / Co)

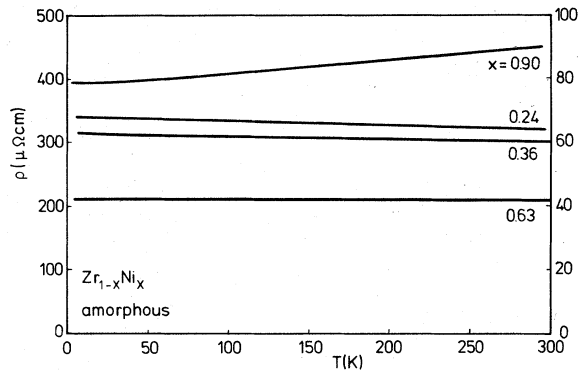


FIG. 3. Temperature dependence of the electrical resistivity in amorphous $Zr_{1-x}Ni_x$ alloys: $x=0.24, 0.36,$ and 0.63 , left-hand scale; $x=0.90$, right-hand scale.

slightly negative temperature coefficient. This is more clearly seen in Fig. 5, where we compare the resistivity ratio $r = [\rho(T) - \rho(300)] / \rho(300)$ for two Zr-rich amorphous alloys. It is seen that both alloys give rise to a small maximum in the low-temperature region.

Inspection of the amorphous alloy ribbons showed that they are not of uniform thickness and breadth. The absolute values of the resistivities are inaccurate for this reason and have to be regarded as upper limits.

IV. DISCUSSION

Amorphous alloys are solid materials in which crystallization has been prevented and the random atomic structure of liquid alloys has been largely retained due to rapid cooling from the melt. In the kinetic approach to glass formation the crystallization rate can generally be described in terms of nucleation and growth.⁶ It can be shown that amorphous alloys can be obtained by means of continuous cooling from the liquid phase if cooling rates are supplied that are sufficiently

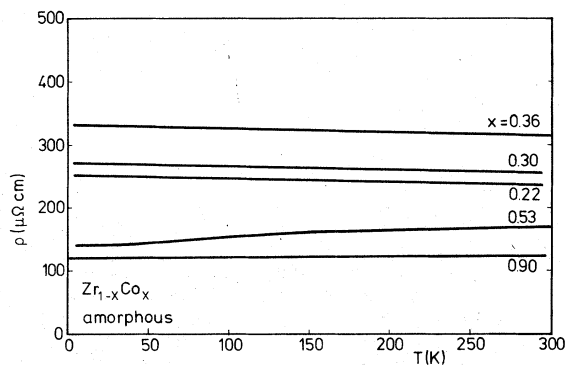


FIG. 4. Temperature dependence of the electrical resistivity in several amorphous $Zr_{1-x}Co_x$.

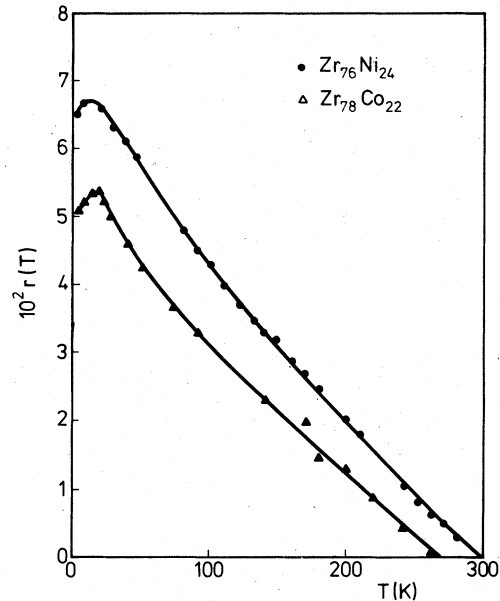


FIG. 5. Temperature dependence of the resistivity ratio $r = [\rho(T) - \rho(300)] / \rho(300)$ of two amorphous Zr-3d metal alloys.

high to bypass the "nose" in the time-temperature transformation (TTT) curve.⁷ It is clear that if the formation of nuclei during the quenching process could have been completely avoided, the thermal stability of the amorphous state would depend in a similar way on the avoidance of the nose region in the TTT diagram upon subsequent thermal treatment. In the case of alloys like the present materials, that cannot be regarded as easy glass formers, the complete absence of nuclei in the amorphous ribbons is unlikely. The thermal stability of the amorphous alloys will therefore primarily be determined by diffusion of the atoms or better by viscous flow.⁸ The temperature dependence of the viscosity (η) is given by

$$\eta = \eta_0 \exp(\Delta E_{\text{act}} / TS_0), \quad (1)$$

where η_0 and ΔE_{act} are constant. The quantity ΔE_{act} is a measure of the potential energy barrier for cooperative atomic transitions. S_0 represents the configurational entropy. This quantity decreases exponentially with temperature below the melting point. At temperatures lower than the glass temperature T_g it adopts very small values and can be regarded as being approximately temperature independent.⁶ The thermal stability of the glass, when expressed in terms of T_g (or its upper limit T_x), is therefore mainly determined by ΔE_{act} . In fact one would expect T_g (or T_x) in all alloys to be proportional to ΔE_{act} .

In close analogy to the importance of the equilibrium concentration of vacancies for diffusion in crystalline solids, we can expect that in the present case ΔE_{act} is for an important fraction accounted for by the enthalpy needed to create a hole as large as a diffusing atom. Then it is relatively easy to understand why the crystallization temperature increases regularly with increasing Ni (or Co) concentration.

In an analysis of the enthalpies of formation of monovacancies, ΔH_{1V} , in pure metals Miedema⁹ has shown that ΔH_{1V} can be introduced as the surface energy of a hole of the size of an atom, multiplied by a correction factor $(n_{\text{WS}}^{1/2} - n_h^{1/2})^2$. Here n_{WS} is the electron density at the boundary of an (unrelaxed) bulk atomic cell and n_h is the electron density at the center of a vacancy. For metallic elements $n_h/n_{\text{WS}} \approx 0.2$ fairly independent of the metal, so that the reduction factor amounts to 0.3. Since the surface energy of Zr is smaller than that of Ni, a hole of the size of a Ni atom will take less enthalpy in pure Zr or in Zr rich alloys than in pure Ni or Ni rich alloys. Relative to the value of ΔH_{1V} in pure Zr, a hole needed for the diffusion of Ni atoms will take less energy because (i) Ni atoms are smaller than Zr atoms ($V_{\text{Ni}}^{2/3}/V_{\text{Zr}}^{2/3} = 0.6$) and (ii) the value of n_h/n_{WS} will become larger than 0.2 in holes surrounded by Zr atoms that are smaller than the Zr atom themselves. A detailed calculation shows that the enthalpy needed to create a hole of the size of a Ni atom is about 108 kJ/mol in pure Ni but only about 67 kJ/mol in pure Zr. In alloys $\text{Zr}_{1-x}\text{Ni}_x$ the formation enthalpy of a hole of the size of a Ni atom can be approached by means of a linear interpolation between these two values, after transforming the concentrations x into effective surface concentrations $xV_{\text{Ni}}^{2/3}/[V_{\text{Ni}}^{2/3} + (1-x)V_{\text{Zr}}^{2/3}]^{-1}$. The values ΔH_h calculated in this way are indicated by the topmost broken line in Fig. 6. In the middle concentration range, in particular, one expects the actual values to be somewhat higher, since no account has been taken yet of the enthalpy of alloying. This excludes a quantitative comparison of the calculated ΔH values with the experimental T_x values, also included in Fig. 6.

Quantitatively one can say, however, that in the range $x < 0.6$ the T_x values measured scale reasonably well to the calculated ΔH_h values. In the region of very high Ni concentration the T_x values adopt considerably lower values than expected, which suggests that here the activation energy is much lower than would correspond to the creation of a Ni hole. In amorphous alloys of sufficiently high Ni content the first crystallizing phase is presumably elementary Ni. Due

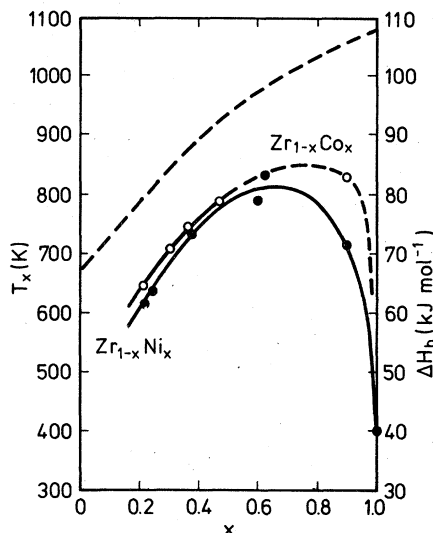


FIG. 6. Concentration dependence of the crystallization temperature T_x (left-hand scale) in $\text{Zr}_{1-x}\text{Ni}_x$ (lowest curve), $\text{Zr}_{1-x}\text{Co}_x$ (middle curve). The T_x value of pure Ni has been taken from Wright (Ref. 26). The topmost broken curve represents the formation enthalpy of a hole of the size of a Ni atom (right-hand scale).

to concentration fluctuations, regions will exist that are void of Zr atoms. It is plausible that crystallization can occur more easily here by means of short-range rearrangements of atoms without the creation of a hole of the size of a whole Ni atom. In this connection it is worth mentioning that the amorphous systems under investigation also show modes of crystallization in which the activation energy is higher than

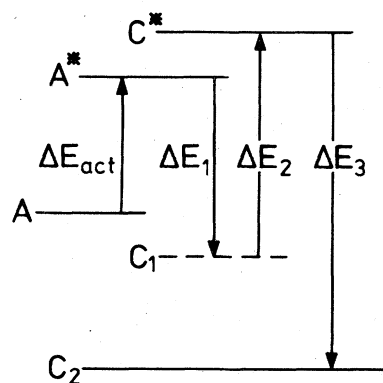


FIG. 7. Possible level scheme of the relative free energies of the amorphous alloy (A), the stable crystalline state (C_2), and a metastable crystalline state (C_1). The activation energy $\Delta E_{\text{act}} = \Delta E(A \rightarrow A^*)$ is involved in the first crystallization step, leading to the metastable state C_1 . In the second step, leading from the metastable state C_1 to the stable state C_2 , the activation energy is $\Delta E_2 = \Delta E(C_1 \rightarrow C_2)$. In general, two steps will occur if $\Delta E_{\text{act}} < \Delta E_2$.

that corresponding to the formation of a Ni hole. This is the case for instance in $Zr_{78}Ni_{22}$, where the crystallization was shown to involve two steps (see Fig. 2). The energy scheme can be represented as in Fig. 7. The free energy of the amorphous state A is higher than that of the two crystalline states C_1 and C_2 . X-ray diffraction has shown that the metastable crystalline state C_1 corresponds to a homogeneous cubic phase, whereas the state C_2 corresponds to the equilibrium condition in the Zr-Ni phase diagram which, in the case of $Zr_{78}Ni_{22}$, entails two separate crystalline phases (α -Zr and Zr_2Ni , see Sec. III). The necessity to achieve separation of phases varying appreciably in Zr concentration makes a long-range diffusion of Ni atoms and possibly also of the larger Zr atoms unavoidable. The activation energy corresponding to the formation of C_2 would therefore be higher than the activation energy $\Delta E_{act} = E(A - A^*)$ corresponding to the formation of C_1 . Preference is therefore given to a crystallization process involving the consecutive steps $A \rightarrow A^*$, $A^* \rightarrow C_1$, $C_1 \rightarrow C^*$, and $C^* \rightarrow C_2$ (see the arrows in Fig. 7).

An impression of the relative positions of the various energy levels involved can be obtained from the specific heat data. In $Zn_{78}Ni_{22}$ the first and second crystallization peak positions (Fig. 2) correspond to ΔE_{act} and ΔE_2 , respectively. The surface area corresponding to these two peaks gives an indication of the differences $\Delta E_1 - \Delta E_{act}$ and $\Delta E_3 - \Delta E_2$. Depending on the magnitude of $\Delta E_1 = \Delta E(A^* \rightarrow C_1)$, the state C^* need not necessarily be higher in energy than the state A .

A satisfactory description of the resistivity behavior of amorphous metals can usually be obtained in terms of quasi-liquid-metal pseudo-potential scattering (Ziman theory¹⁰ and extensions¹¹⁻¹⁵). The resistivity (ρ) is given by

$$\rho = \frac{12\pi\Omega_0}{e^2\hbar v_F} \int_0^1 S(q)|t(q)|^2 \left(\frac{q}{2k_F}\right)^3 d\left(\frac{q}{2k_F}\right), \quad (2)$$

where v_F and k_F are the Fermi velocity and Fermi wave vector, q is the scattering vector, Ω_0 is the atomic volume, and S the structure factor of x-ray interference function. The single-site t matrix can usually be expressed in terms of phase shifts. Due to the q^3 factor, the integral of Eq. (2) heavily weights the values of the integrand close to $q = 2k_F$. For this reason the temperature dependence of ρ is primarily determined by the temperature dependence of $S(q \approx 2k_F)$. It can be shown that at temperatures comparable to or higher than $\Theta/2$ (Θ is the Debye temperature) ρ is linear in T . In the case where the electron concentration in the alloy is such that $q = 2k_F$ coincides (or nearly coincides) with the main peak ($q = Q_p$) in

the interference function the temperature coefficient of the resistivity (TCR) is negative. This is a direct consequence of the broadening of the interference function with increasing temperature, which lowers all values near $q = Q_p$ (TCR < 0) but raises all values further away from the center of the main peak (TCR > 0). On the basis of this approach it is therefore possible to obtain information about k_F by means of the sign of TCR. We have plotted the experimental X-ray scattering vectors of the main peak maximum (Q_p) in various $Zr_{1-x}Co_x$ and $Zr_{1-x}Ni_x$ alloys in Fig. 8. The values of the pure elements are taken from the literature.^{16,17} It is seen that the Q_p is a smooth function of x , increasing almost linearly from the value of Q_p in Zr to those in Ni or Co. The k_F value of these alloys can be obtained in the free electron model by means of the expression

$$k_F = (3\pi^2 N \bar{D} \bar{Z} / A)^{1/3}, \quad (3)$$

where N is Avogadro's number, \bar{A} and \bar{Z} are the weighted atomic weight and weighted number of valence electrons, respectively. For the density \bar{D} we used the weighted density of the pure elements. The electrical conductivity in the amorphous alloys is mainly determined by the s elec-

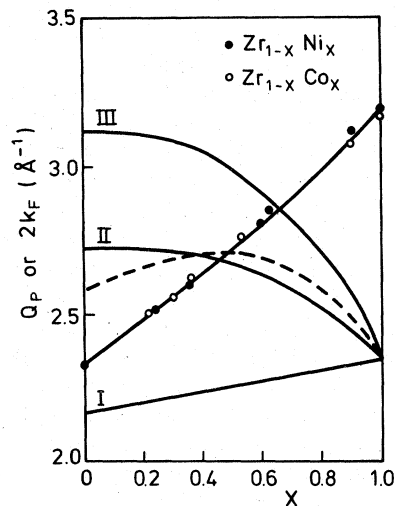


FIG. 8. Concentration dependence of the scattering vector $Q_p = 4\pi \sin \Theta / \lambda$, corresponding to the main peak in the x-ray interference function (full line through data points.) The concentration dependence of $2k_F$ has been calculated assuming Zr atom contributions of 1, 2, and 3 valence electrons (curves I, II, and III, respectively). The broken line has been calculated with an effective valence of 1.7 of the Zr atoms but including the effect of transfer of charge [$\Delta z = (1-x)P\Delta\phi^*/2$] from Zr 4d to Ni 4s. The value of \bar{Z} used in Eq. (3) is now $\bar{Z} = (1-x)1.7 + 0.6x + \frac{1}{2}x(1-x)P\Delta\phi^*$, where $\Delta\phi^* = 2.2$ eV and $P = 0.7$ were taken from the data listed by Miedema (Ref. 19).

trons. Due to the comparatively high effective mass of the d electrons their contribution to the electrical conductivity is considerably lower. The k_F values we are interested in should therefore pertain to s -type electrons. Each of the $3d$ transition-metal atoms (Ni, Co) contributes about 0.6 s electrons.¹⁸ The number of s electrons contributed by the Zr atoms (Z_{Zr}) is less well established. We have calculated the concentration dependence of $2k_F$ therefore in the cases where Zr contributes one to three s electrons (curves I–III in Fig. 8). The condition for the occurrence of a negative TCR is reached when the $2k_F$ curve intersects the Q_p curve in Fig. 8. Actually negative TCR's can be expected for $q = 2k_F$ values in the immediate vicinity of Q_p . Taking account of the width of the main peaks (Fig. 1) it seems reasonable to extend the q region in which $TCR < 0$ to about 0.15 \AA^{-1} on either side of the Q_p curve in Fig. 8. With this assumption only curve II in Fig. 8 gives rise to a concentration region with $TCR < 0$ that would reasonably match with experimental observation: It can be seen in Fig. 3 that the values of TCR are negative in the range $0.24 \leq x \leq 0.63$ in the case of $Zr_{1-x}Ni_x$.

It cannot be excluded that there is transfer of charge from the Zr atoms to the $3d$ atoms. For this reason we have included in Fig. 8 (broken line) the concentration dependence of $2k_F$ calculated for the case of transfer of 0.8 electrons from Zr to Ni.¹⁹ In the same manner as argued above it follows from the concentration dependence of the Q_p curve and the broken line in Fig. 8 that a negative TCR is expected in the range $0.2 < x < 0.6$. It can be concluded therefore that also in the case charge transfer effects would be operative the extended Ziman model can satisfactorily explain the negative TCR observed in the range 20–60-at. % Ni.

It was shown in Sec. III that several of the Zr-rich amorphous alloys have a positive TCR at very low temperatures ($T < 20$ K), changing to a negative TCR at higher temperatures. This effect is not well understood at present. We can rule out the explanation that the decrease of ρ with T below 20 K is the result of magnetic ordering, since the Ni atoms do not carry a moment in this concentration range. The most likely explanation can be given in terms of a model due to Cote and Meisel¹⁵ who considered elastic and inelastic (phonon scattering) contributions of $S(q)$ separately. Numerical estimates made by Cote and Meisel show the heights of these maxima to be of the order of tenths of a percent, which would agree with the results shown in Fig. 5. From Figs. 3 and 4 it can be derived that the absolute magnitude of the resistivity is rather high in

$Zr_{76}Co_{22}$ ($250 \mu\Omega \text{ cm}$) and even higher in $Zr_{76}Ni_{24}$ ($330 \mu\Omega \text{ cm}$). These values seem to preclude a mean free path sufficiently long for a dominant phonon contribution at low temperatures. It was mentioned, however, in Sec. III that considerable error may be involved in the absolute values of the resistivities due to the not uniform thickness and breadth of the amorphous ribbons.

The occurrence of a negative TCR is a rather uncommon feature in metallic systems. In crystalline materials it is often attributed to Kondo exchange scattering or Mott s - d scattering. The former is magnetic in origin and highly concentration-dependent, the latter is sensitive to the shape of the $3d$ electron band in the region around the Fermi energy. Both these explanations can be excluded in the present case on the grounds of the insensitivity of the negative TCR to variations of x in $Zr_{1-x}M_x$ on the one hand and to variations of M (Ni, Co) on the other. It is surprising that negative TCR's occur relatively often in metallic glasses. Presumably this is closely connected with the relatively high stability of the amorphous state with respect to the crystalline state in alloys satisfying the condition $2k_F \approx Q_p$. The stability criterion $2k_F \approx Q_p$ of Nagel and Tauc²³ has recently been looked upon in a different way. Beck and Oberle²⁴ argue that in the case $2k_F \approx Q_p$ there is a close match between the atomic pair correlation function and the pair potential in a manner such that most of the successive neighbors of a given atom are located in the consecutive minima of the pair potential. Since these arguments are equally well applicable to the liquid state, the occurrence of relatively stable amorphous $A_{1-x}B_x$ is linked to the occurrence of deep eutectics at the corresponding x values. Each of these two features favors the formation of amorphous alloys by means of continuous quenching from the melt. In the first place the energy of the amorphous state (indicated by A in Fig. 7) is lowered relative to C_2 . If one assumes that the activated state A^* remains more or less in position, this leads to a larger ΔE_{act} and thus to higher glass or crystallization temperatures. In the second place the deepness of the eutectic corresponds to a low melting temperature T_m . It can be shown that the critical cooling rate for glass formation decreases with increasing T_g/T_m ratio.^{6,25} For compositions x at which $2k_F \approx Q_p$ the combination of a relatively high T_g and low T_m cause this ratio to be low and glass formation can be expected to proceed relatively easily.

An estimate of the T_g/T_m ratios of the present materials can be obtained by considering T_x as an upper limit of T_g . These ratios are included in Table I. They fall in the range 0.49–0.63.

The relative lowering of the energy of the amorphous state in the case $2k_F \approx Q_p$ and the accompanying increase of T_x offers a reasonable way of explaining why the correspondence between T_x and ΔH_h is lost when $x > 0.6$ (see Fig. 6). It can be seen in Fig. 8 that in this very concentration range the $2k_F$ curve starts to bend away from the Q_p curve, leading to a higher relative energy for the amorphous state. The much stronger decrease at the highest Ni concentration

has already been discussed above.

ACKNOWLEDGMENTS

The authors wish to thank H.-J. Güntherodt and H. Beck for fruitful discussions. The experimental assistance of P. Hokkeling, J. C. A. Dekker, and W. W. van den Hoogenhof is gratefully acknowledged.

-
- ¹For a review see J. J. Gilman, *Phys. Today* **28**, 46 (1975) and furthermore the various contributions in the books: *Rapidly Quenched Metals*, edited by N. J. Grant and B. C. Giessen (MIT, Cambridge, Mass., 1976); *Metallic Glasses*, edited by J. J. Gilman and H. J. Leamy (American Society for Metals, Cleveland, 1977); *Amorphous Magnetism*, edited by R. A. Levy and R. Hasegawa (Plenum, New York, 1977).
- ²*Constitution of Binary Alloys*, 1st supplement, edited by R. P. Elliot (McGraw-Hill, New York, 1965).
- ³K. H. J. Buschow, M. Brouha, J. W. M. Biesterbos, and A. G. Dirks, *Physica B* **91**, 261 (1977).
- ⁴N. Heiman and N. Kazama, *Phys. Rev. B* **17**, 2215 (1978).
- ⁵J. Chappert, R. Arrese-Boggiano, and J. M. D. Coey, *J. Magn. Magn. Mater.* **7**, 175 (1978).
- ⁶For a review see H. A. Davies, *Phys. Chem. Glasses* **17**, 159 (1976).
- ⁷D. R. Uhlmann, *J. Non-Cryst. Solids* **7**, 337 (1972).
- ⁸S. Takayama, *J. Mater. Sci.* **11**, 164 (1976).
- ⁹A. R. Miedema, *Z. Metallkde* (to be published).
- ¹⁰J. M. Ziman, *Philos. Mag.* **6**, 1014 (1961).
- ¹¹R. Evans, D. A. Greenwood, and P. Lloyd, *Phys. Lett. A* **35**, 57 (1971).
- ¹²O. Dreirach, R. Evans, H.-J. Güntherodt, and H.-V. Künzi, *J. Phys. F* **2**, 709 (1972).
- ¹³S. R. Nagel, *Phys. Rev.* **16**, 1694 (1977).
- ¹⁴P. J. Cote and L. V. Meisel, *Phys. Rev. Lett.* **40**, 1586 (1978).
- ¹⁵P. J. Cote and L. V. Meisel, in *Rapidly Quenched Metals III*, edited by B. Cantor (The Metals Society, London, 1978).
- ¹⁶G. S. Cargill III, *Solid State Phys.* **30**, 227 (1975).
- ¹⁷Y. Waseda and M. Ohtani, *Z. Phys. B* **21**, 229 (1975).
- ¹⁸H.-J. Güntherodt, H. U. Künzi, M. Liard, R. Müller, R. Oberle, and H. Rudin, *Inst. Phys. Conf. Series* **30**, 342 (1977).
- ¹⁹A. R. Miedema, *J. Less-Common Met.* **32**, 117 (1973); **46**, 67 (1976).
- ²⁰S. L. Altman and C. J. Bradley, in *Soft X-ray Band Spectra*, edited by D. J. Fabian (Academic, London, 1968).
- ²¹Y. Waseda and H. S. Chen, *Phys. Status Solidi B* **87**, 777 (1978).
- ²²K. H. J. Buschow, A. M. van Diepen, N. M. Beekmans, and J. W. M. Biesterbos, *Solid State Commun.* **18**, 181 (1978).
- ²³S. R. Nagel and J. Tauc, *Phys. Rev. Lett.* **35**, 380 (1975).
- ²⁴H. Beck and R. Oberle, in Ref. 15.
- ²⁵D. Turnbull, *Contemp. Phys.* **10**, 473 (1969).
- ²⁶J. G. Wright, *IEEE Trans. Magn.* **12**, 95 (1976).